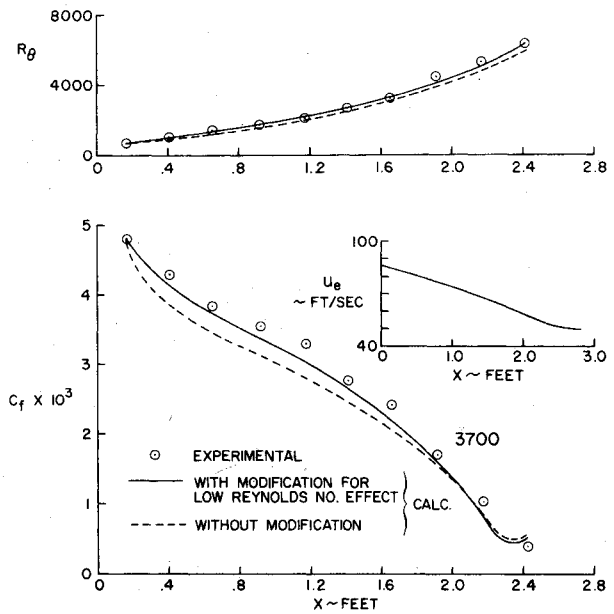

Fig. 6 Calculated and experimental results for case 3700 (data of Moses).

Comparison with Experiment

Figures 1–6 show a comparison of the calculated results with the experiment. The experimental data considered here correspond to the low Reynolds numbers given in Ref. 5. The calculations were made by using the method of Ref. 6, which for incompressible flows consists of solving Eqs. (2) and (3) together with the continuity equation. The method is applicable to both laminar and turbulent boundary layers. The calculations can be started either at the leading edge or at some downstream location. In the former case, the flow starts as laminar and becomes turbulent at any specified x-location by activating the eddy-viscosity expressions. In the latter case, it is necessary to specify the initial velocity profiles.

Figures 1–3 show the calculated and experimental results in which the calculations were started at the leading edge. In these calculations at first an effective length that matched the initial experimental momentum thickness was calculated. For flat-plate flows or flows with initially negligible pressure gradient, this procedure is a satisfactory one. Figure 1 compares the calculated c_f-values with those given by Coles' prediction[7] and the experimental values of Wieghardt.[5] Figure 2 shows the results for Schubauer and Klebanoff's airfoil-like body designated as 2100 in Ref. 5. It is seen that with the low Reynolds number correction, when the experimental R_θ is matched, the skin-friction coefficient is matched also. Figure 3 shows the results for an accelerating flow designated as 1300 in Ref. 5. Again when R_θ is matched, the skin-friction coefficient is also matched.

Figures 4–6 show the calculated and experimental results in which the calculations were started with the experimental initial velocity profile. Calculations were made for various flows with pressure-gradients designated as 2700, 2800, 3100, 3200, 3700, 4000 and 4100 in Ref. 5. As the results show, in all cases the Reynolds-number correction to the calculated results seems to improve the agreement with experiment.

References

[1] Coles, D. E., "The Turbulent Boundary Layer in a Compressible Fluid," Rept. P-2417, 1961, Rand Corp., Santa Monica, Calif.

[2] Cebeci, T., "The Behavior of Turbulent Flow Near a Porous Wall With Pressure Gradient," *AIAA Journal*, Vol. 8, No. 12, Dec. 1970, pp. 2152–2156.

[3] Van Driest, E. R., "On Turbulent Flow Near a Wall," *Journal of Aerospace Science*, Vol. 23, No. 11, Nov. 1956, pp. 1007–1011.

[4] Simpson, R. L., Kays, W. M., and Moffat, R. J., "The Turbulent Boundary Layer on a Porous Plate: An Experimental Study of the Fluid Dynamics With Injection and Suction," Rept. HMT-2, 1967, Stanford Univ., Stanford, Calif.

[5] Coles, D. E. and Hirst, E. H., eds., *Proceedings of the Computation of Turbulent Boundary Layers*, Stanford Univ., Vol. II, 1969.

[6] Cebeci, T. and Smith, A. M. O., "A Finite-Difference Method for Calculating Compressible Laminar and Turbulent Boundary Layers," *Journal of Basic Engineering*, Vol. 92, No. 3, Sept. 1970, pp. 523–535.

[7] Coles, D. E., "Measurements in the Boundary Layer on a Smooth Flat Plate in Supersonic Flow. I. The Problem of the Turbulent Boundary Layer," Rept. 20-69, June 1953, Jet Propulsion Lab., Pasadena, Calif.

Solar Electron Temperatures and X-Ray Flare Activity

D. M. Horan* and R. W. Kreplin†
Naval Research Laboratory, Washington, D. C.

Parameters of Solar X-Ray Source Regions

X-RAYS, especially in the shorter wavelengths, are not uniformly emitted from the solar disk, but have discrete, active regions as sources. Therefore, changes in the magnitude or spectral character of the solar energy flux must be associated with changes in the solar source regions.

The predominant source mechanisms for continuum solar x-ray emission are free-free (bremsstrahlung) transitions and free-bound (radiative recombination) transitions. Equations describing such transitions[1] show that the electron concentration, volume, and electron temperature associated with the source region are parameters which would affect the magnitude and spectral character of the solar x-ray emission. It is possible to use a pair of broad-band x-ray sensors to measure changes in these parameters and a brief outline of the technique follows.

The current generated in an ionization chamber is given by[2]

$$I = Ae\omega\int\epsilon(\lambda)E(\lambda,T)d\lambda \qquad (1)$$

where e is the electronic charge, ω is the number of ion pairs produced in the gas per unit of absorbed energy, A is the effective window area of the detector, $E(\lambda,T)$ is the solar emission spectrum, λ is the wavelength, T is the electron temperature, $\epsilon(\lambda)$ is the efficiency of the detector, and the integration is performed over wavelengths where ϵ is nonzero. If two ionization chambers sensitive to slightly different portions of the x-ray band are used, the ratio of the currents generated will be dependent on the electron temperature through the solar emission spectrum, $E(\lambda,T)$. If the solar emission spectrum is due to bremsstrahlung and radiative recombination, we are able to express it in the form

$$E(\lambda,T) = C(\lambda,T)\int N_e^2 dV \qquad (2)$$

Presented as Paper 70-1371 at the AIAA Observation and Prediction of Solar Activity Conference, Huntsville, Ala., November 16–18, 1970; submitted January 15, 1971; revision received March 26, 1971. The authors acknowledge the support of the Naval Air Systems Command under NAVAIR Air Task Number A3705381 652B 1F01551701, SOLRAD (Solar Radiation). Also, the authors gratefully acknowledge the assistance of K. P. Dere who spent a considerable amount of time searching for suitable data and converting it into a computer-compatible form.

* Research Physicist, E. O. Hulburt Center for Space Research.
† Head, Solar Radiation Section, Upper Air Physics Branch.

where N_e is the electron concentration and V is the volume of the source region. The temperature dependence of the ratio of the currents generated in two different x-ray detectors can then be expressed as

$$r(T) = \frac{\omega_1 A_1 \int \epsilon_1(\lambda) C(\lambda,T) d\lambda}{\omega_2 A_2 \int \epsilon_2(\lambda) C(\lambda,T) d\lambda} \quad (3)$$

in which we have assumed that $\int N_e^2 dV$, the emission measure, is identical for both bands. This assumption becomes less valid as the x-ray bands considered in the ratio become more separated in wavelength. The detector characteristics, ω, A, and ϵ, are known and we can calculate values for $C(\lambda,T)$ over an expected range of temperatures. Therefore, a comparison of the experimentally measured ratio of the currents generated in two detectors with the calculated values for $r(T)$ can give us an electron temperature T_s associated with the source region.

Once the electron temperature associated with the source region has been determined, the emission measure associated with the source region can also be obtained. The calculated values of $C(\lambda,T)$ are used in the equation

$$I/\int N_e^2 dV = e\omega A \int \epsilon(\lambda) C(\lambda,T) d\lambda = G(T) \quad (4)$$

to obtain the detector current per unit emission measure, $G(T)$, as a function of temperature. Therefore, the emission measure associated with the source region is given by

$$\int N_e^2 dV = I/G(T_s) \quad (5)$$

where I is the current produced in the detector. If an x-ray photograph of the sun is available the volume associated with the active region can be estimated and an average value for the electron concentration can then be extracted from the emission measure. The technique for obtaining a source temperature and emission measure is covered in much greater detail in a recent paper by Horan.[3]

Application of Technique

If x-ray data of sufficient continuity are available, a source region's electron temperature and emission measure can be obtained as functions of time. Figure 1 is a plot of these parameters associated with the source region of an x-ray flare which occurred on October 22, 1967. The detectors used to evaluate the parameters were the ionization chambers sensitive to the 0.5–3 Å and 1–8 Å bands which were included in the NRL experiment aboard NASA's OGO-4 satellite. The lowest data curve on the plot shows the energy flux measured by the 0.5–3 Å ionization chamber and presents the time profile of the flare's x-ray emission. The conversion from detector current to energy flux assumed a ten million degree gray-body[2] solar emission spectrum. The top data curve shows the electron temperature, to the nearest million degrees, obtained from the ratio of the detector currents, assuming that the solar continuum emission was due to bremsstrahlung and radiative recombination. The middle data curve shows the calculated emission measure. The error bars

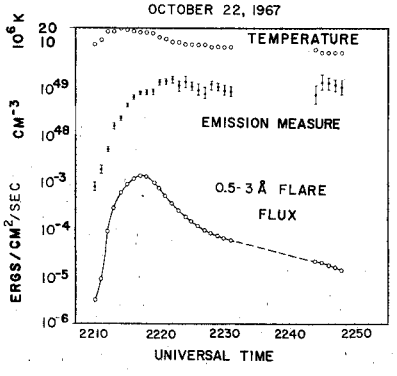

Fig. 1 Electron temperature and emission measure variations during a solar x-ray flare.

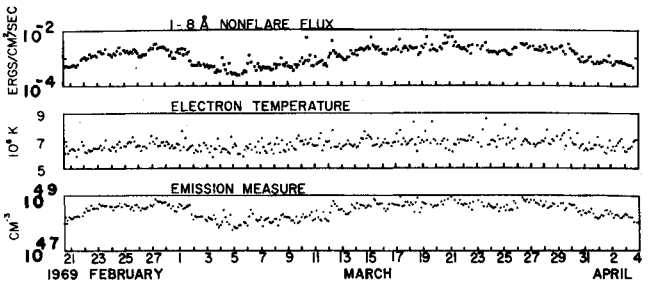

Fig. 2 Electron temperature and emission measure derived from nonflare x-ray flux.

indicate the range of values for the emission measure when the temperature was allowed to vary by ±0.5 million degrees about the determined electron temperature. The plot shows that changes in the temperature and emission measure of a source region during the course of a flare are significant.

Changes in the nonflare solar x-ray emission must also correspond to changes in the electron temperature and emission measure of the source region. Figure 2 shows the electron temperature and emission measure for periods when no flares were in progress, between February 21 and April 4, 1969. Data from the 1–8 Å and 0.5–3 Å ionization chambers included in the NRL experiment aboard NASA's OSO-5 satellite were used. The detector responses when no flares were in progress, and the electron temperatures and emission measures obtained from these nonflare responses, were averaged in three hour blocks, and the average values obtained were plotted. The top data line on the plot shows the 1–8 Å nonflare flux averages in units of ergs/cm²/sec. The conversion from detector current to energy flux assumed a two million degree gray-body solar emission spectrum. The middle curve shows the electron temperature of the x-ray source region in millions of Kelvin degrees. A conservative correction for amplifier noise was made to each of the detector currents before taking the current ratio used to determine the electron temperature. The lowest data curve shows the calculated emission measure in units of cm^{-3}.

The periods when the average 1–8 Å nonflare flux exceeds 1.0×10^{-3} ergs/cm²/sec closely correspond to periods of enhanced x-ray flare activity between February 22 and March 1, when the 1–8 Å band flare flux exceeded 1×10^{-2} ergs/cm²/sec seventeen times and 1×10^{-1} ergs/cm²/sec four times; and between March 9 and March 30, when the 1–8 Å band flare flux exceeded 1×10^{-2} ergs/cm²/sec forty-four times and 1×10^{-1} ergs/cm²/sec seven times. The 1–8 Å band flux exceeded 1×10^{-2} ergs/cm²/sec on only four other occasions during the period covered by Fig. 2. The electron temperature and emission measure curves also show changes which correspond to the amount of flare activity, but the changes in the electron temperature may be moderated and the changes in the emission measure may be magnified by the inability to completely correct the 0.5–3 Å data for amplifier noise contributions. The low 0.5–3 Å background flux on February 21, between March 2 and March 10, and after March 30 causes detector currents which are just slightly above the noise level of the amplifiers. Therefore, amplifier noise causes the measured 0.5–3 Å background flux to be too large by a significant percentage. Since the 1–8 Å background flux causes detector currents well above the amplifier's noise level, the noise error in the 0.5–3 Å flux measurements causes the electron temperature to be overestimated. An overestimation of the electron temperature leads to an underestimation of the emission measure. The noise corrections applied to the data are believed to be conservative, and if this is so, the true range of the electron temperature variation with flare activity would be greater than that shown in Fig. 2.

No electron temperature determination could be made for times prior to February 21 and after April 4 because the 0.5

–3 Å flux was below the sensitivity threshold of the experiment on OSO-5. During the only other periods when the background 0.5–3 Å flux was found to be above the threshold level, June 1–June 17, 1969, November 17–30, 1969, and February 1–4, 1970, electron temperatures were found to be in the seven–eight million degree range during periods of flare activity.

The 0.5–3 Å experiment designed for SOLRAD 10, which is to be launched in 1971, will be approximately six times more sensitive than the OSO-5 experiment. Hopefully, it will significantly increase the periods when background 0.5–3 Å flux is measurable and enable a better assessment of the variation of nonflare electron temperatures with flare activity to be made.

References

[1] Culhane, J. L., "Thermal Continuum Radiation from Coronal Plasmas at Soft X-Ray Wavelengths," *Monthly Notices of the Royal Astronomical Society*, Vol. 144, No. 3, 1969, pp. 375–389.

[2] Kreplin, R. W., "Solar X-Rays," *Annales de Geophysique*, Vol. 17, No. 2, April-June 1961, pp. 151–161.

[3] Horan, D. M., "Coronal Electron Temperatures Associated With Solar Flares," Ph.D. dissertation, 1970, Catholic Univ. of America; also Publication 70-22133, University Microfilms Inc., Ann Arbor, Michigan.

Hypersonic Limits for Laminar, Constant–Pressure Boundary Layers

MERWIN SIBULKIN*

Brown University, Providence, R. I.

Nomenclature

$(c_f)_e;(c_f)_r$ = $\tau_w/\frac{1}{2}\rho_e u_e^2$; = $\tau_w/\frac{1}{2}\rho_r u_e^2$, friction coefficients
c_p = specific heat
k_{eq} = equilibrium thermal conductivity
M = Mach number
n = 0 for planar flow, = 1 for axisymmetric flow
p = static pressure
Pr_{eq} = $\mu c_p/k_{eq}$
q = heat flux
$Re_e;Re_r$ = $\rho_e u_e x/\mu_e$; = $\rho_r u_e x/\mu_r$, Reynolds numbers
$st_e;st_r$ = $q_w/\frac{1}{2}\rho_e u_e^3$; = $q_w/\frac{1}{2}\rho_r u_e^3$, Stanton numbers
u,v = velocity components parallel and normal to body
x,y = coordinates parallel and normal to body
γ = ratio of specific heats
μ = viscosity
ρ = density
τ = shear stress

Subscripts

e = boundary layer edge value
r = reference state
w = wall value

Introduction

IN this note the laminar boundary layer problem is formulated in such a way that the skin friction parameter and Stanton number parameter approach constant values for Mach numbers much greater than one. The results obtained provide a rapid method of estimating skin friction and heat transfer for $M_e > 10$.

Received February 19, 1971; revision received April 12, 1971. This work was partially supported by the National Science Foundation through Grant GK-16535.

Index Category: Boundary Layers and Convective Heat Transfer—Laminar.

* Professor of Engineering. Associate Fellow AIAA.

Analysis

In the low speed limit $M_e \to 0$, it is well known that the friction and heat-transfer parameters for laminar flow over an insulated flat plate approach constant values. This result is emphasized in Fig. 1a by plotting the von Kármán and Tsien[1] result for $\mu \propto T^{0.76}$, $Pr = 1.0$ on semi-logarithmic coordinates. As M_e increases, one notes that $(c_f)_e\, Re_e^{1/2}$ and $st_e Re^{1/2}$ decrease continually. However, in the high-speed limit $M_e \gg 1$ (or $M_e^{-1} \to 0$) it may be possible to obtain "hypersonic limits" for these parameters. Such an analysis is given below for laminar, constant pressure (i.e., flat plates, wedges, cones) boundary layers.

The boundary layer equations for constant pressure

$$(\rho u r^n)_x + (\rho v r^n)_y = 0 \tag{1}$$

$$\rho u u_x + \rho v u_y = (\mu u_y)_y \tag{2}$$

$$\rho u h_x + \rho v h_y = [(k_{eq}/c_p)h_y]_y + \mu u_y^2 \tag{3}$$

are transformed by defining the coordinate transformations

$$\eta \equiv \frac{u_e r^n}{(2\zeta)^{1/2}} \int_0^y \rho dy^*, \quad \zeta \equiv \int_0^x \rho_r \mu_r u_e r^{2n} dx^* \tag{4}$$

and a nondimensional stream function

$$f \equiv \psi/(2\zeta)^{1/2} \tag{5}$$

Equation (4) is identical to the Levy-Lees transformation except for the introduction of "reference values" of ρ and μ defined by

$$\rho_r = \rho(h_r, p_e) \qquad \mu_r = \mu(h_r, p_e) \tag{6}$$

where the reference enthalpy $h_r = \frac{1}{2}u_e^2$. After defining the nondimensional variables

$$\tilde{u} = u/u_e, \quad \tilde{h} = h/h_r, \quad \tilde{\rho} = \rho/\rho_r, \quad \tilde{\mu} = \mu/\mu_r \tag{7}$$

and substituting Eqs. (4–7) into Eqs. (1–3), the boundary-layer equations may be written as

$$[\tilde{\rho}\tilde{\mu}\tilde{u}']' + f\tilde{u}' = 0 \tag{8}$$

$$[(\tilde{\rho}\tilde{\mu}/Pr_{eq})\tilde{h}']' + f\tilde{h}' + 2\tilde{\rho}\tilde{\mu}(\tilde{u}')^2 = 0 \tag{9}$$

where

$$f = \int_0^\eta \tilde{u} d\eta^*$$

and $(\ )'$ indicates differentiation with respect to η. It should be noted that Eq. (9) has no explicit Mach number dependence. The boundary conditions (for a constant temperature wall) are

$$\begin{aligned} &\text{at } \eta = 0; \quad f = 0, \quad \tilde{u} = 0, \quad \tilde{h} = \tilde{h}_w \\ &\text{at } \eta = \infty; \qquad \tilde{u} = 1, \tilde{h} = \tilde{h}_e \end{aligned} \tag{10}$$

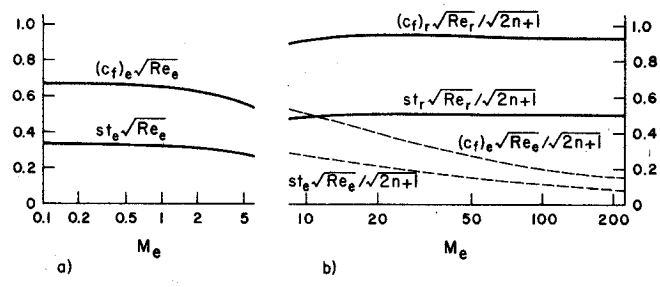

Fig. 1 Low Mach number and high Mach number limits for the friction and heat transfer parameters.